RSC Publishing Faraday Discussions

Probing solvation and reactivity in ionized polycyclic aromatic hydrocarbon-water clusters with photoionization mass spectrometry and electronic structure calculations.

Journal:	*Faraday Discussions*
Manuscript ID	FD-ART-12-2018-000229.R1
Article Type:	Paper
Date Submitted by the Author:	18-Jan-2019

Complete List of Authors:	Xu, Bo; Lawrence Berkeley National Laboratory, Chemical Sciences Division Stein, Tamar ; UC Berkeley Ablikim, Utuq; E O Lawrence Berkeley National Laboratory, Chemical Dynamics; Kansas State University, Physics Jiang, Ling; Dalian Institute of Chemical Physics, State Key Laboratory of Molecular Reaction Dynamics Hendrix, Josie; University of California - Berkeley, Chemistry Head-Gordon, Martin; University of California - Berkeley, Chemistry Ahmed, Musahid; Lawrence Berkeley National Laboratory, Chemical Sciences Division

Probing solvation and reactivity in ionized polycyclic aromatic hydrocarbon-water clusters with photoionization mass spectrometry and electronic structure calculations.

Bo Xu[1@], Tamar Stein[2#@], Utuq Ablikim[1], Ling Jiang[3], Josie Hendrix[2], Martin Head-Gordon[1,2] & Musahid Ahmed[1*]

1 Chemical Sciences Division, Lawrence Berkeley National Laboratory, Berkeley, CA, 94720, USA

2 Department of Chemistry, University of California, Berkeley, CA, 94720, USA

3 State Key Laboratory of Molecular Reaction Dynamics, Dalian Institute of Chemical Physics, Chinese Academy of Sciences, 457 Zhongshan Road, Dalian 116023, P. R. China

[@] Equal contributions.

Present address: Fritz Haber Research Center for Molecular Dynamics, Hebrew University of Jerusalem, Jerusalem 9190401, Israel

Abstract

Polycyclic Aromatic Hydrocarbons (PAHs) may comprise up to 20% of the carbon budget in our galaxy and most PAHs condense onto the water-rich icy grain mantles. Benzene-water clusters have been invoked as model systems to study the photo-processing of water ice mantles containing PAHs. However, there is a paucity of information on larger aromatics, where the extended π cloud could affect photo-processing. In this study, tunable vacuum ultraviolet (VUV) photoionization of naphthalene-water clusters $N_x(H_2O)_y$ (N denotes naphthalene) are performed using synchrotron radiation and analyzed by reflectron time-of-flight mass spectrometry. Naphthalene clusters up to x=4 are generated as are naphthalene-water clusters up to y=25. At low photon energy (< 11 eV), the naphthalene moiety is ionized and there is no proton transfer from N^+ to water sub-cluster, which is very different from the benzene-water system. Protonated products, $N[(H_2O)_xH]^+$ and OH radical addition product $(NOH)[(H_2O)_xH]^+$ are generated above 11 eV, suggesting that water sub-clusters dominate the dynamics at high photon energies. Ab-initio calculations are performed to decipher the experimental results. Energetics of the neutral structures $N(H_2O)_{1-4}$ and their photoionized counterparts are calculated, including ionization on N moiety as well as on the water sub-cluster. Energy decomposition analysis (EDA) is performed to understand trends in the binding between the naphthalene and the water sub-cluster in the ionized species.

1. Introduction

In cold interstellar regions, icy mantles form on dust grains, and polycyclic aromatic hydrocarbons (PAHs) can freeze out on them.[1] UV and VUV processing can occur on these ices. The subsequent photochemistry can be ion or radical mediated, giving rise to possibly complex new molecules via dehydrogenation and charge or proton transfer occuring after the initial ionization event.[2-5] Clusters are a convenient model to study PAH-water interactions. There have been many experimental and theoretical studies of neutral and ionized forms for the hydration of the smallest aromatic, benzene. Early work has been reviewed by Mons et al,[6] and recent experimental work, particularly IR and electronic spectroscopy of cations, can be found in the papers of Miyazaki et al.[7-9] Prakash et al. provides a comprehensive review of the spectroscopy of benzene-water clusters in the neutral state.[10] Ibrahim et al. discuss the mechanism of deprotonation that occurs in Benzene$^+$$(H_2O)_x$ (x >= 4) clusters using ion mobility measurements coupled with theoretical thermodynamic arguments.[11] Both Miyazaki and Ibrahim suggest that hydration of benzene cation leads to its deprotonation, giving rise to a phenyl radical and hydrogen bonded to a protonated water sub-cluster.[7, 11]

In contrast to benzene, there have been far fewer experimental and theoretical studies of larger PAHs with water.[12-15] El Shall's group used ion mobility mass spectrometry coupled with density functional theory (DFT) to study the thermodynamics of naphthalene-water clusters.[16] For these systems, they postulated that there is external solvation of the hydrocarbon, and chains mediated by C-H interactions are formed upon clustering. No evidence of deprotonation of the naphthalene cation was observed. Using ion flow methods, Bierbaum[17] showed that there was no reaction between the naphthalene cation and water, but reaction with naphthyl radical was facile. Vibrational and electronic spectroscopy revealed that in the protonated naphthalene-water monomer, the proton is located in naphthalene; however, the process is dramatically reversed with the addition of a second water.[18] Infrared dissociation spectroscopy[19-20] and theoretical calculations[21-23] suggest that water clusters tend to maximize the number of intra-cluster hydrogen bonds and form a cyclic network sitting on the PAH surface.

PAH-water clusters are being investigated for use in a variety of applications. These systems may serve as useful models for understanding water-graphite and water-graphene interactions,[24] driven by significant societal interest in water purification and hydrogen production within the

confinement of carbon nanotubes. It has been suggested that water exhibits increased structural order in nano-confined geometries.[25] Another area of speculation lies in how aromatic systems with π clouds[26] can be used for molecular recognition,[27] which is of interest in both sensing and medical technologies.

It has been suggested that PAH ionization energies (IEs) are lowered upon being embedded in water ice, which allows UV photons to initiate photoionization.[28] Woon et al.[29] calculated IE's for benzene and naphthalene solvated by one water, and also embedded in ice. Their results showed a substantial lowering of PAH ionization energies upon interaction with water. To date, there have not been direct measurements of naphthalene-water photoionization in the gas phase to benchmark against theoretical predictions and validate these early experimental measurements performed on naphthalene-water clusters.[30] Moreover, as the number of water molecules in a naphthalene-water cluster increases, there is an increase in the scope for interesting structural rearrangements to stabilize the positive charge upon ionization, as well as increased potential for reactive chemical events to occur upon ionization. With these possibilities in mind, we present synchrotron-based VUV photoionization mass spectrometry measurements on naphthalene-water clusters generated in a supersonic expansion molecular beam coupled with electronic structure calculations to elucidate the effect of water on the photoionization dynamics of naphthalene and its clusters. We will compare our results to those from the benzene-water system to highlight the drastically altered photoionization dynamics upon addition of a second ring to benzene.

2. Methods

2.1 Experimental methods

The experiments are performed with a reflectron time-of-flight mass spectrometer incorporating a continuous supersonic expansion molecular beam source. The apparatus is coupled to a 3 meter vacuum monochromator on the Chemical Dynamics Beamline (9.0.2) located at the Advanced Light Source and has been described in our previous studies.[31] Briefly, naphthalene was placed at the front end of a stainless-steel nozzle, which has a 50 μm diameter center hole, and is heated to 328 K using a cartridge heater. Naphthalene vapor is diffused into 800 Torr argon carrier gas seeded with water vapor. The gas mixture passes through the 50 μm hole and expands

supersonically in vacuum to produce a molecular beam at the interaction region of a reflectron time-of-flight mass spectrometer where the neutral clusters are ionized by the VUV light and subsequently detected. Mass spectra are recorded for the photon energy range between 8 and 12.5 eV in photon energy step size of 50 meV. The photoionization efficiency (PIE) curves of the water clusters are obtained by integrating over the peaks in the mass spectrum at each photon energy, and are normalized by the photon flux.

2.2 Theoretical Methods

All calculations reported in this manuscript were carried out using Q-Chem.[32] Structures and relative energies were calculated using density functional theory (DFT). Specifically, geometry optimization of the neutral and cation structures was carried out using the ωB97X-V functional[33] with the cc-pVTZ basis set. ωB97X-V is a range separated functional and as such reduces the self-interaction error; it is thus useful for the treatment of radical cations.[34] Moreover, it contains non-local Van der Waals correlation via the VV10 functional[35] to accurately describe noncovalent interactions and thus is also suitable to study naphthalene water clusters. In two separate large-scale benchmarking exercises,[36] ωB97X-V was ranked as the top-performing hybrid generalized gradient approximation functional.

To directly assess the validity of ωB97X-V for the naphthalene-water cations studies here, binding energies were computed for several isomers of $N^+(H_2O)$ characterized recently by Chatterjee et al.[19,20] These calculations used the aug-cc-pVTZ basis set. Two more recent functionals formulated by Mardirossian and Head-Gordon, the Rung 4 range-separated hybrid, ωB97M-V and the Rung 5 double hybrid ωB97M(2)[37] are compared against ωB97X-V, B3LYP, and B3LYP-D3(0) in Table 1. Binding energies computed for monohydrated N^+ complexes using the ωB97X-V functional (Table 1) were found to be in good agreement with those obtained using B3LYP-D3 by Chatterjee et al,[20] as well as those obtained with the more accurate ωB97M-V and ωB97M(2) functionals. Unsurprisingly, use of the uncorrected B3LYP functional leads to significant underbinding of 1.5-2 kcal/mol due to neglect of dispersion effects.

Table 1: Calculated binding energies (kcal/mol) using the aug-cc-pVTZ basis for monohydrated naphthalene cation complexes at optimized structures reported in ref. 20.

	M18	M12	M23	M(π)
B3LYP-D3	-9.42	-8.32	-7.96	-6.60
B97M-V	-9.03	-7.96	-7.63	-6.90
B3LYP	-7.80	-6.76	-6.44	-4.25
ωB97X-V	-9.23	-8.13	-7.74	-6.60
ωB97M-V	-9.21	-8.15	-7.75	-6.73
ωB97M(2)	-9.61	-8.38	-7.98	-6.97

We studied both neutral and ionized clusters. When the clusters are ionized, the charge can be either on the naphthalene part or on the water part, depending on the energy of the photon. While calculations involving the cation where the charge lies on the naphthalene are straight forward, calculating the cation where the charge is on the water sub-cluster is more complex as this is not the ground state of the system. In order to successfully converge to a state where the charge remains on the water moiety, we partitioned the system into fragments using constrained locally-projected SCF for molecular interactions (SCF-MI) procedure available in Q-Chem.[36-37] In SCF-MI the occupied molecular orbitals on each fragment are expanded in terms of atomic orbitals of the fragments. The resulting MOs are localized on the fragments and called absolutely localized molecular orbitals (ALMOs).[38-39] We used a fragment method based on locally projected equations by Stoll et. al.[40] Due to the constraint, the calculation resulted in the charge on the water cluster. We then ran another calculation in which the starting guess of the SCF was the constrained calculation, and in order to help the calculation converge we used the maximum overlap method (MOM)[41] to preserve the initial orbitals, with the charge staying on the water sub-cluster. After converging with the MOM we again read the SCF-guess and converged the calculation with direct inversion of the iterative subspace (DIIS) as usual.

3. Results

3.1. Overview of Experimental Results

3.1.1 Mass spectra The mass spectra of $[N_x(H_2O)_y]^+$ clusters generated at photo energies of 10 and 12.5 eV are shown in Figure 1a and 1b, respectively. There are four series of naphthalene-water clusters $[N(H_2O)_{0\text{-}25}]^+$, $[N_2(H_2O)_{0\text{-}10}]^+$, $[N_3(H_2O)_{0\text{-}7}]^+$, and $[N_4(H_2O)_{0\text{-}4}]^+$ at 10 eV (Figure 1a), shown in black, red, blue and green color, respectively. There are also $[N(Ar)_{1\text{-}3}]^+$ clusters generated (pink peaks), suggesting that the molecular beam after supersonic expansion is cold. At a photon energy of 12.5 eV (Figure 1b), the pure water clusters $[(H_2O)_xH]^+$ appear (cyan peaks) as the water clusters begin to be ionized around 11 eV.[42]

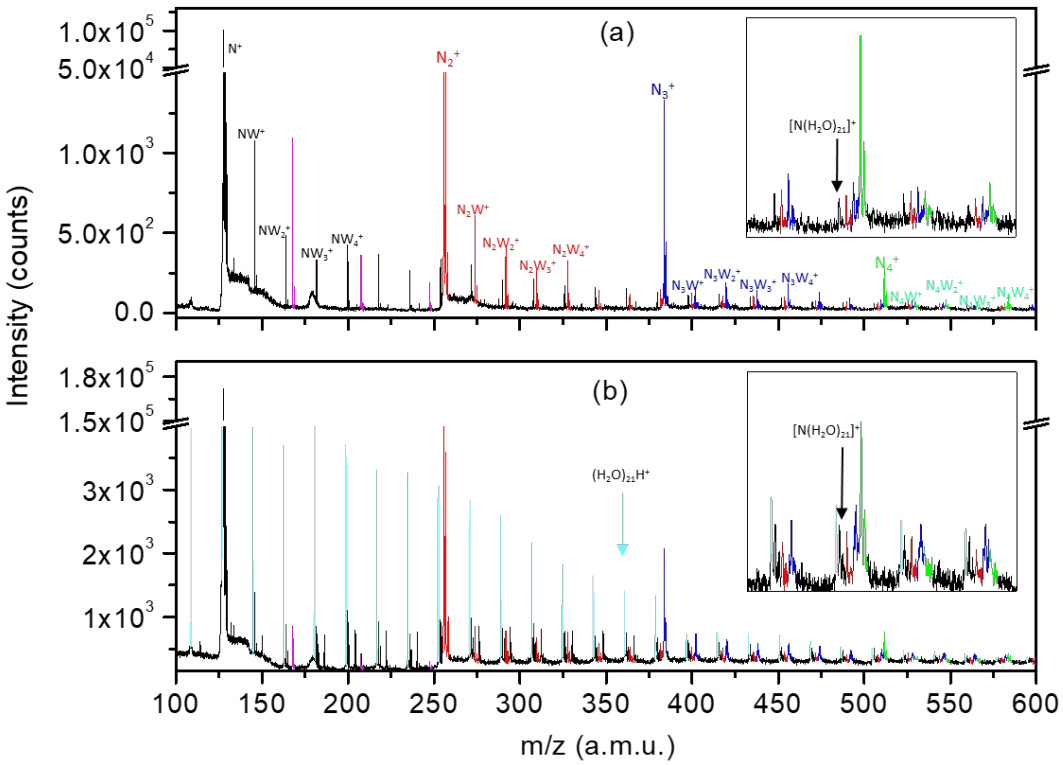

Figure 1. Time-of-flight mass spectra of naphthalene-water clusters at (a) 10 eV and (b) 12.5 eV. $N_xW_y^+$ denotes $[N_x(H_2O)_y]^+$. The inset shows the region at mass to charge (m/z) 520 corresponding to $[N(H_2O)_{20\text{-}24}]^+$. The cyan arrow indicates $(H_2O)_{21}H^+$ while the black arrows indicate $[N(H_2O)_{21}]^+$.

3.1.2 Photoionization efficiency (PIE) curves

The photoionization efficiency (PIE) curves of $[N_x(H_2O)_y]^+$ are shown in Figure 2. Using a non-linear least squares fitting technique, we derive their appearance energies (AE) from their PIE curves and provide them in Table 2. The PIE curve of N monomer overlaps very well with our previous

study[43] (Figure 2a) recorded on pure naphthalene monomer using the same apparatus. The AE of naphthalene monomer obtained in our experiment (8.15 ± 0.05 eV) is very close to that obtained from two-color two-photon experiment (8.136 eV)[44] while the AEs of $N_{2\text{-}4}$ clusters are higher than those obtained in Ref. 44. Note that there is a blue shift of 0.10 eV for the AE of $[N(H_2O)_1]^+$ relative to that of N. A blue shift of 0.09 eV was also observed for anthracene/$[anthracene(H_2O)_1]^+$ system[45] while there was a red shift of 0.08 eV for benzene/$[benzene(H_2O)_1]^+$ system.[46] The blue shift for $[N(H_2O)_1]^+$ and $[anthracene(H_2O)_1]^+$ may be due to larger structural change after ionization compared to $[benzene(H_2O)_1]^+$ and is discussed later.

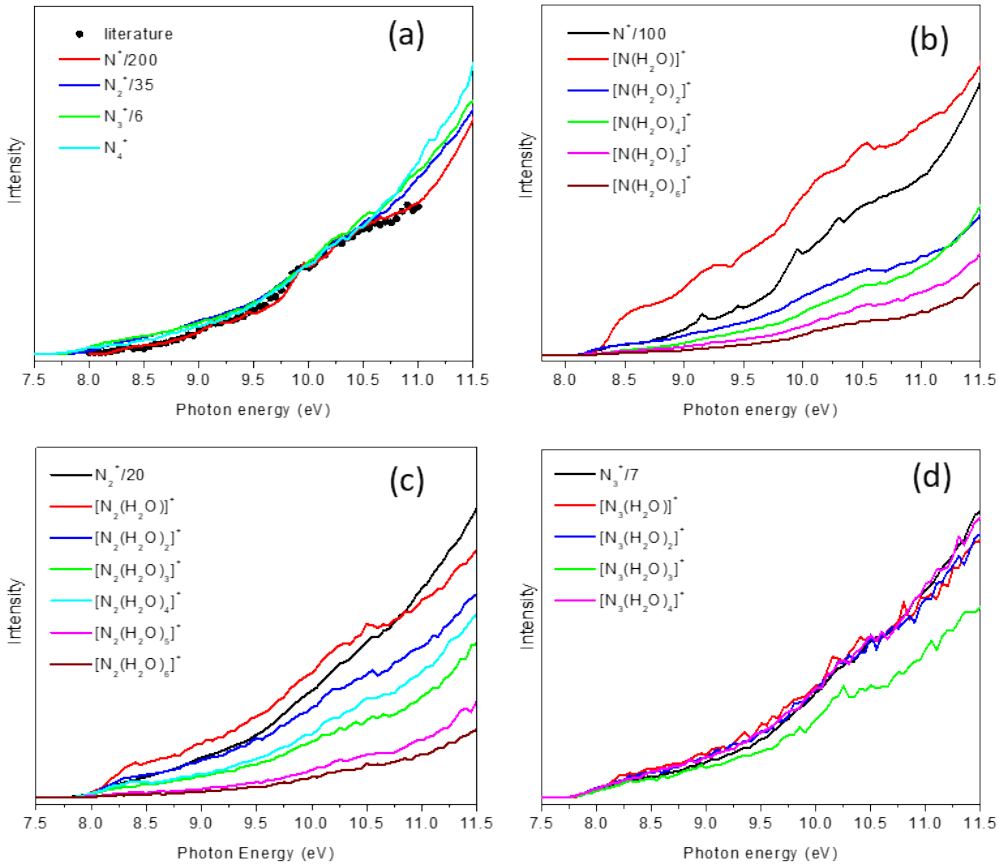

Figure 2. PIE curves of (a) $N_{1\text{-}4}^+$, (b) $[N(H_2O)_{0\text{-}6}]^+$, (c) $[N_2(H_2O)_{0\text{-}6}]^+$, and $[N_3(H_2O)_{0\text{-}4}]^+$ from 7.5 to 11.5 eV. The intensities of N^+, N_2^+ and N_3^+ are divided by 1400, 140, and 15 in Figure 2a, respectively. The intensities of N^+, N_2^+ and N_3^+ are divided by 100, 20, and 7 in Figure 2b, 2c, and 2d, respectively.

Table 2. The appearance energies (AE) of N_{1-4}^+, $[N(H_2O)_{0-6}]^+$, $[N_2(H_2O)_{0-6}]^+$, $[N_3(H_2O)_{0-4}]^+$ clusters and the calculated adiabatic and vertical ionization energies (AIEs and VIEs) of $[N(H_2O)_{1-4}]^+$.

N_x	AE (eV)	$[N(H_2O)_x]^+$	AE	AIE	VIE	$[N_2(H_2O)_x]^+$	AE	$[N_3(H_2O)_x]^+$	AE
N	8.15	$[N(H_2O)]^+$	8.25	7.87	8.40	$[N_2(H_2O)]^+$	7.95	$[N_3(H_2O)]^+$	7.83
N_2	7.90	$[N(H_2O)_2]^+$	8.12	7.57	8.50	$[N_2(H_2O)_2]^+$	7.95	$[N_3(H_2O)_2]^+$	7.75
N_3	7.75	$[N(H_2O)_3]^+$	8.25	7.73	8.40	$[N_2(H_2O)_3]^+$	7.90	$[N_3(H_2O)_3]^+$	7.83
N_4	7.67	$[N(H_2O)_4]^+$	8.20	7.61	8.26	$[N_2(H_2O)_4]^+$	7.87	$[N_3(H_2O)_4]^+$	7.75
		$[N(H_2O)_5]^+$	8.12			$[N_2(H_2O)_5]^+$	7.90		
		$[N(H_2O)_6]^+$	8.15			$[N_2(H_2O)_6]^+$	7.95		

3.2 Calculated structures for neutral and ionized clusters

We started by studying the structures of neutral naphthalene water clusters with up to 4 water molecules. All the neutral structures presented here are minima on the potential energy surface (PES) and exhibit only positive eigenvalues of the force constant matrix in the frequency calculations. In the neutral states, the orientation of the water clusters can be either on top of the aromatic ring (Figure 3a-d), or side-on to the ring (Figure 3e-h). In the “top” configuration, the interaction is mainly between the hydrogens of the water and the π cloud of the naphthalene, while in the “side” configuration, the interaction is between the oxygen of the water and the hydrogens of the naphthalene. The top configuration is generally more stable than the side configuration, except in the case of $N(H_2O)_2$. From Figure 3, it is clear that the tendency of water molecules is to cluster, and the structure of the water sub-cluster is similar to the structures found in isolated water clusters.[14]

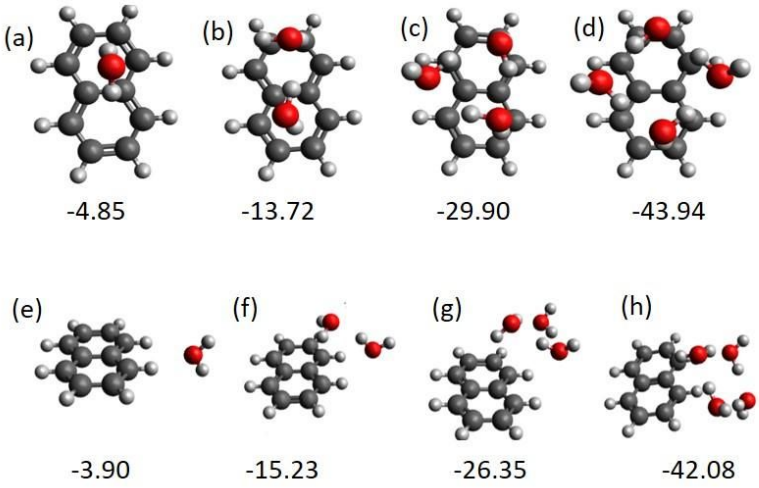

Figure 3. Top: neutral clusters with water sub-cluster "on top" of the naphthalene ring. Bottom: Neutral cluster with the water sub-clusters "side" to the naphthalene ring. The binding energies (BE) in kcal/mol of the two configurations of the water-naphthalene clusters are given below the structure. The BE of $N(H_2O)_x$ was calculated as follows, $BE[N(H_2O)_x] = E[N(H_2O)_x] - E[N] - x\ E[H_2O]$.

We next calculated the structure of cationic clusters after ionization of the naphthalene moiety. In the case of the ionized clusters, we also found two main classes of stable configurations. While there can be other (meta-)stable structures, we focus on these two configurations as they are the adiabatic states of the cation complex directly accessed starting from the neutral structures discussed above. In the first class of configurations, the water molecules remain on top of the aromatic ring as in the neutral cluster, but since the naphthalene moiety now is positively charged, the water molecules flip such that the oxygen is pointing towards the naphthalene as can be seen in Figure 4(a)-(d). This leads to favorable charge-dipole interactions, as well as polarization and some charge transfer between the oxygen atoms and naphthalene cation. The interactions in the ionized clusters between naphthalene and the water sub-cluster will be discussed in detail later. The second class of configurations, previously been discussed in Ref. 16, involve the coordination of a “side chain” of water molecules to ionized naphthalene, as can be seen in the bottom panel of Figure 4.

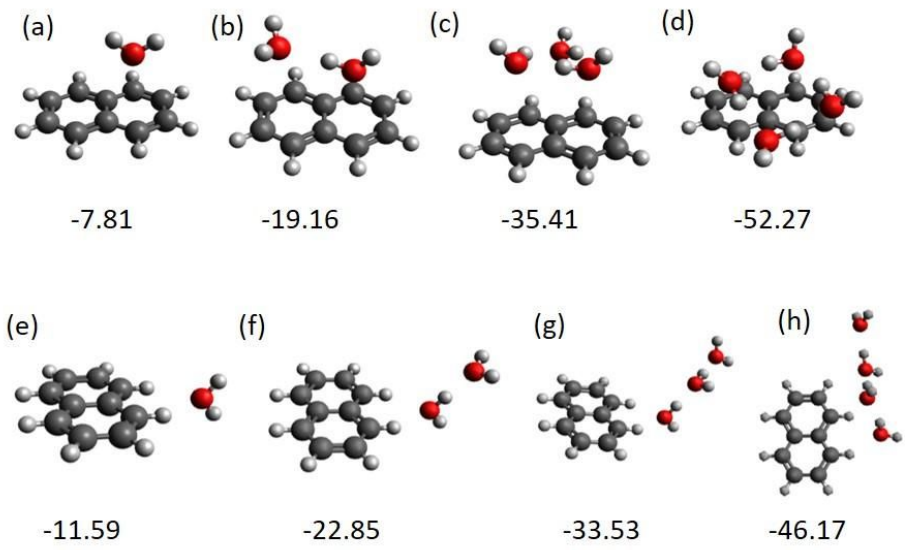

Figure 4. Ionized clusters with the charge on the naphthalene part. Upper panel: "top" configurations, with the water molecules oriented so that the partially negative oxygen atoms and their lone pairs are pointing toward the positively charged naphthalene. Bottom panel: Side chain configurations. The binding energies (BE) in kcal/mol of the two configurations of the water-naphthalene clusters are given below each structure. BEs are calculated as follows: $BE[N^+(H_2O)_x] = E[N^+(H_2O)_x] - E[N^+] - x\ E[H_2O]$.

If the ionizing photon is sufficiently energetic, the water moiety can be the site of the initial ionization, rather than naphthalene. Figure 5 shows the structures that result from ionization of the water sub-cluster. Figure 5(a) presents the adiabatic structure for the case of one water molecule, meaning this is the structure resulting from relaxation of the neutral structures on the cationic surface. Unlike the case where the naphthalene is being ionized, here we see that the water does not flip and the structure resembles that of the neutral one. Figure 5(b) to 5(f) presents the structures for the case of two, three and four water molecules respectively. Here we observe the previously documented characteristics of ionized water clusters.[34, 47-51] Ionized dimer water clusters are known to form what are known as the 'hemi-bond' and 'proton transfer' structures. These structures can be identified upon ionization of the water sub-cluster in the naphthalene water complex. In Figure 5(b) the structure is the well-known hemi-bonded structure, while Figure 5(c) shows a proton transfer structure. In the case of two water molecules, the proton transfer structure is the adiabatic configuration. For the case of three water molecules, the adiabatic

structure resembles the hemi-bond structure. In the case of four water molecules shown in Figure 5(e), one can see an OH^- H^+ separation where the H^+ is shared between two water molecules; this is the adiabatic structure. Figure 5(f) shows the case of a hemi-bond like structure for a four-water molecule cluster.

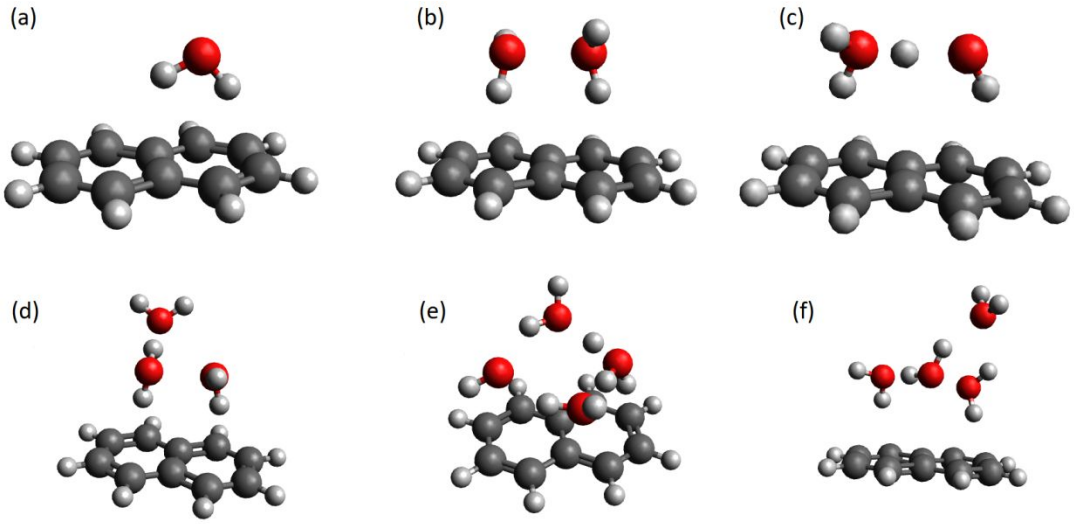

Figure 5. Adiabatic structures with the water sub-cluster being the ionized moiety. Note the presence of hemi-bonded structures (e.g. (b), (f)), as well as proton transferred structures (e.g.(c)).

3.3 Photoionization of $N(H_2O)_x$ below 11 eV

In this study, $N(H_2O)_x$ clusters started to appear around 8.20 eV, which is very close to the ionization energy of naphthalene. As a result, we can suspect that the character of the ionized state of naphthalene moiety in $N(H_2O)_x$ remains the same as in the isolated naphthalene. Once an electron is emitted from the naphthalene moiety, $N^+(H_2O)_x$ clusters are generated. In contrast to mass spectra of cationic benzene-water clusters,[52] there is no magic number (x = 21) observed in Figure 1, which is always observed upon ionization of bare water clusters, suggesting that there is no proton transfer from N^+ moiety to $(H_2O)_x$ sub-cluster. Our result is consistent with the results reported in an infrared photodissociation (IRPD) spectroscopy study,[20] where combined with DFT calculations, it is indicated that there is no intracluster proton transfer for $N^+(H_2O)_x$ when x <= 5. Our study suggested that there is no proton transfer even for clusters of size x = 25.

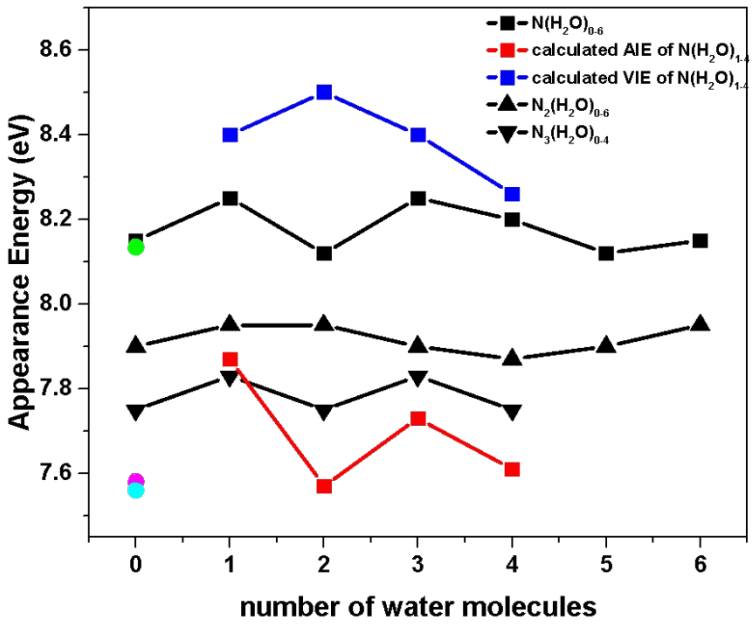

Figure 6. Measured AEs of $N(H_2O)_{0\text{-}6}$, $N_2(H_2O)_{0\text{-}6}$, and $N_3(H_2O)_{0\text{-}4}$. Calculated AIEs and VIEs of $N(H_2O)_{1\text{-}4}$. The appearance energies of N, N_2 and N_3 from Reference 36 are shown with green, magenta and cyan circles, respectively.

We also calculated the adiabatic ionization energy (AIE) and vertical ionization energy (VIE) of $N(H_2O)_{1-4}$. Table 2 and Figure 6 give the experimental appearance energies and theoretical ionization energies. As mentioned, there is a drop in the appearance energy measurement for bare naphthalene clusters starting from 8.15 eV, and again at 7.90, 7.75, and 7.67 eV with subsequent additions of naphthalene. In contrast, there is an oscillation of appearance energies measured with the addition of waters to the naphthalene monomer and higher clusters. Theoretical calculations for water clustering with the naphthalene monomer show a similar trend, presented in Figure 6, suggesting that structural rearrangements upon ionization are affecting the measured appearance energies. Upon close observation of the PIE curves shown in Figure 2, it is apparent that the addition of one water to naphthalene changes the Franck Condon envelope dramatically, evidenced by resulting shifts of the PIE curve. With addition of subsequent waters, the spectra slowly begin to resemble naphthalene again. This trend is also apparent in the $N_2(H_2O)_x$ series with a somewhat diminished effect, and has all but disappeared for the naphthalene trimer.

3.4 Ionization above 11 eV

3.4.1 Proton transfer

As shown in Figure 1a, the intensity of the peak at m/z $N(H_2O)_x$+1 (x >=2) relative to the peak at m/z $N(H_2O)_x$ retains the natural ^{13}C isotope abundance (about 11%) at 10 eV while it increases at 12.5 eV (Figure 1b). The $[N(H_2O)_x+1]^+/[N(H_2O)]^+$ ratio exhibits a clear onset (followed by a sharp rise) at around 11 eV (Figure 7b), which can be used to separate the contribution of ^{13}C isotope abundance and proton transfer within the same mass channel. For example, the onsets of $[N(H_2O)+1]^+/[N(H_2O)]^+$ and $[N(H2O)_2+1]^+/[N(H_2O)_2]^+$ are 11.75 and 11.20 eV, respectively, which are nearly the same as the appearance energies of $[(H_2O)H]^+$ and $[(H_2O)_2H]^+$,[42] respectively. As presented in Figures 3-5, theoretical calculations suggest that water molecules in $N(H_2O)_x$ tend to form a hydrogen bonded sub-cluster above the naphthalene ring, and the structure of this water sub-cluster is similar to those found in isolated water clusters. Judging from the similar structures and AE, we suspect that the water sub-clusters in naphthalene-water clusters are ionized at the photon energies described above. The increase of the peak intensity at m/z $N(H_2O)_x + 1$ indicates

there is proton transfer within the water sub-clusters and subsequent elimination of OH radical, as shown in equation 1.

$$N(H_2O)_{x+1} + h\nu \rightarrow N[(H_2O)_xH]^+ + OH \quad (x >= 2) \qquad (1)$$

An isotopic experiment using D_2O was conducted and the mass spectra at 10 eV and 12.5 eV are given in Figure 8 below. The appearance of peaks at m/z $[N(D_2O)_x]^+$+2 confirmed the proton transfer channel. Consequently, photoionization and proton transfer processes of water sub-clusters in $[N(H_2O)_x]$ are very similar to those of pure water clusters $(H_2O)_x$, and the N moiety is likely an spectator with little influence on the photoionization and proton transfer process of water sub-clusters in $[N(H_2O)_x]$. This phenomenon was also observed in the microsolvation of acenaphthene. The microwave and far-infrared spectra of acenaphthene–water clusters show that the water sub-clusters are locked, and retain most of the pure water cluster characteristics with negligible perturbation by the PAH.[14-15]

The proton transfer induced by the ionization of the water moiety was also observed in a previous photoionization study of microhydrated 1,3-dimethyluracil (mU) clusters from our group.[53] The proton transfer channel opened up when the lowest ionized state of solvated water corresponding to an excited ionized state of the $mU(H_2O)_n$ cluster (3A") became accessible. In contrast to the current study, the ionized states localized on water are affected largely by the interaction with mU and the onsets of proton transfer are independent of the cluster size. Due to the high proton affinity of mU compared with water, the proton bonds to only one oxygen atom of the mU.

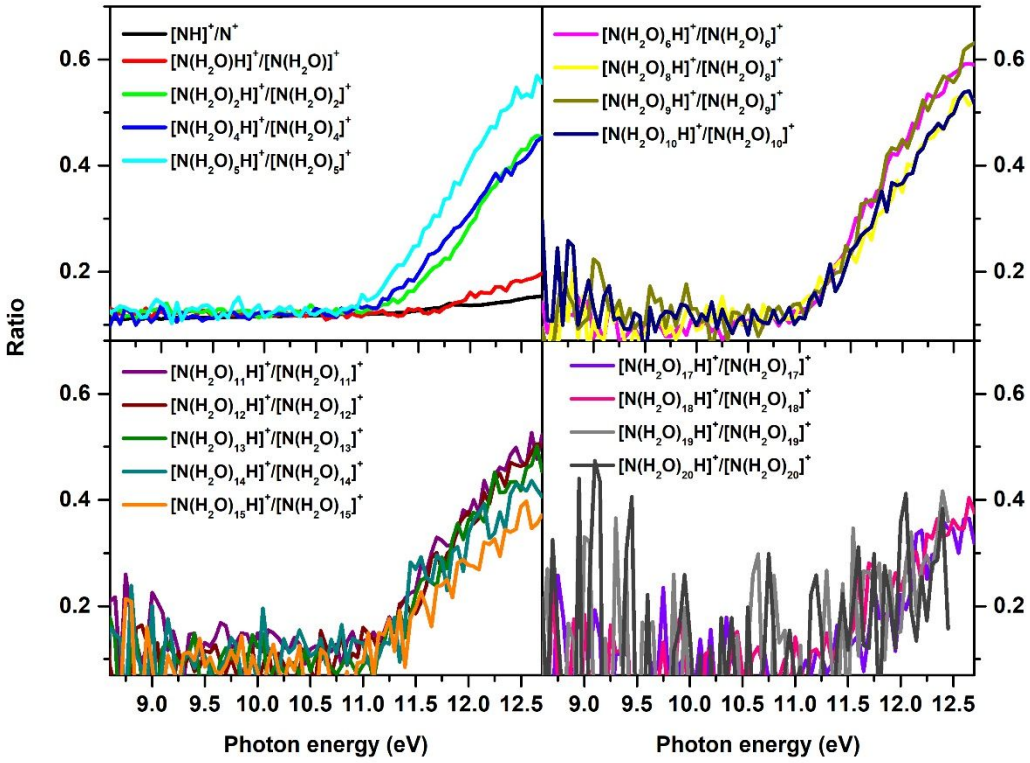

Figure 7. The intensity ratios of $[N(H_2O)_x+1]^+/[N(H_2O)_x]^+$ at different photon energies.

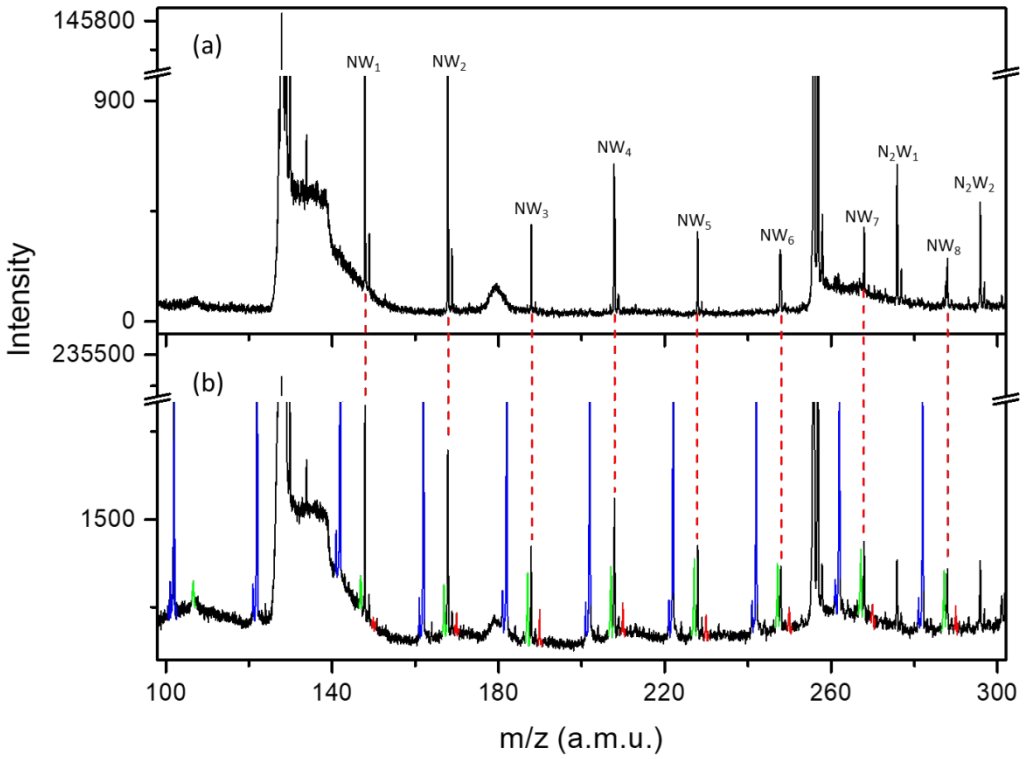

Figure 8. Time-of-flight mass spectra of $[N_x(D_2O)_y]^+$ (N denotes naphthalene) clusters at (a) 10 eV and (b) 12.5 eV. $N_xW_y^+$ denotes $[N_x(D_2O)_y]^+$. The peaks at m/z $[N(D_2O)_y]$+2 are shown in red. $(D_2O)D^+$ clusters are shown in blue and their metastable fragments are shown in green.

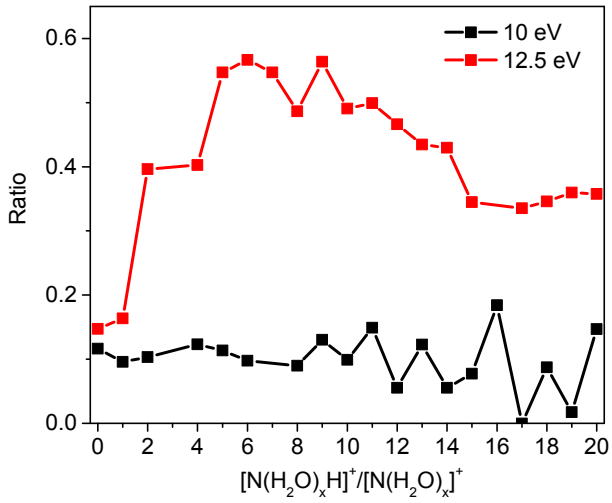

Figure 9. The intensity ratios of $[N(H_2O)_x+1]^+/[N(H_2O)_x]^+$ as a function of cluster size at 10 and 12.5 eV.

The intensity ratios of $[N(H_2O)_x+1]^+/[N(H_2O)_x]^+$ as a function of cluster size at 10 and 12.5 eV are given in Figure 9. At 10 eV, there is no change of intensity with cluster size. In contrast, the intensity of $[N(H_2O)_x+1]^+/[N(H_2O)_x]^+$ increases with cluster size at 12.5 eV, reaches the maximum at around x = 5 – 9, and then decreases for larger clusters. The peak of proton transfer around 5-9 waters and subsequent decrease for the larger clusters could be due to a number of factors. With an increase of the number of waters, other channels for fragmentation could be opening up, or the rate of proton transfer could be decreasing with an increase in cluster size. Our own study of pure water cluster fragmentation and proton transfer do not show such behavior upon ionization between 11-12.5 eV, which highlights that the addition of even a single naphthalene molecule to a water cluster can induce dramatic changes in the fragmentation dynamics.

Table 3. Calculated VIEs and AIEs of $N(H_2O)_{1-4}$ upon ionization of water sub-clusters.

$N(H_2O)_x$	VIE (eV)	AIE(Hemi-bonded)	AIE(proton- transfer)
$N(H_2O)$	11.74		11.45
$N(H_2O)_2$	10.92	9.76	9.60
$N(H_2O)_3$	11.13	9.51	8.0
$N(H_2O)_4$	11.11	9.27	9.12

Calculations of the energetic pathways upon ionization of the water moiety suggest that ionization is occurring from the 3A" state of water, and provides for very interesting dynamics with the addition of subsequent waters. There is no proton transfer upon ionization of the NW dimer; however, as shown in Table 3, it becomes quite clear that the VIE is tracking ionization of pure water clusters and matches our experimental onsets very well. If one pays close attention to the AIE, the energetics of the final proton transferred states decrease in the following manner: 11.45, 9.60, 9.51, and 9.12 eV with addition of 1, 2, 3 and 4 water molecules respectively. This would suggest that there will be internal energies of 0.29, 1.32, 1.61 and 1.99 eV in the ionized system which can give rise to proton transferred and hemi-bonded structures along the ionizing potential energy surface. The hemi-bonded states will not be observable in our experiment, though future spectroscopy experiments might be able to capture these transient structures.

3.4.2 OH addition

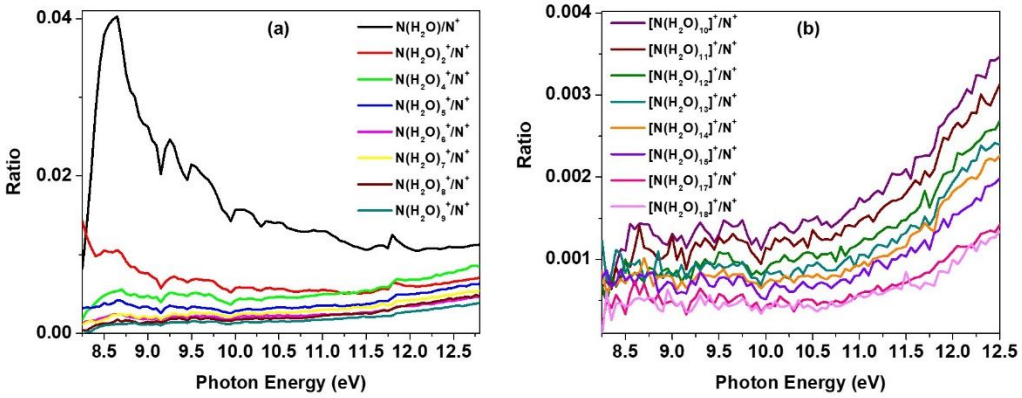

Figure 10. (a) The intensity ratio of $[N(H_2O)_{1\text{-}9}]^+/N^+$ versus photon energies; (b) The intensity ratio of $[N(H_2O)_{10\text{-}18}]^+/N^+$ versus photon energies.

We also compared the effect of water on the ionization efficiency of $N(H_2O)_x$ by dividing the PIE curve of $[N(H_2O)_x]^+$ by that of N^+. The $[N(H_2O)_x]^+/N^+$ ratio (Figure 10) becomes flat when cluster size grows below 11 eV, which means the PIE curves of $[N(H_2O)_x]^+$ start to resemble that of naphthalene. The $[N(H_2O)_x]^+/N^+$ ratio starts to increase at around 11 eV. As discussed above, water sub-cluster is ionized around 11 eV. The increase of this ratio indicates that the ionization of water sub-clusters can contribute to the generation of $[N(H_2O)_x]^+$. Different from the generation of $N[(H_2O)_xH]^+$, the generation of $[N(H_2O)_x]^+$ means the OH group is not emitted after water ionization. There have been several gas-phase studies on the reaction between OH radical and naphthalene, and two main reaction channels are identified: OH addition and H-atom abstraction reactions at C1 and C2 positions of naphthalene.[54-56] The OH radical addition dominates at low temperature and the lifetime of the OH-naphthalene adduct is estimated to be 1000 seconds.[55] As a result, we can suspect that the OH radical reacts with naphthalene after ionization of water sub-cluster in $N(H_2O)_{x+1}$, and $(NOH)[(H_2O)_xH]^+$ is generated, as shown in equation (2).

$$N(H_2O)_{x+1} + h\nu \rightarrow (NOH)[(H_2O)_xH]^+ \quad (x >= 2) \qquad (2)$$

There is no $(N\text{-}H)(D_2O)_xD^+$ generated in the isotope experiment using D_2O, which means no H-atom abstraction reaction occurs.

We calculated the vertical and adiabatic ionization of water sub-clusters in $N(H_2O)_{3-4}$ (Figure 11). The vertical ionization energies of $N(H_2O)_{3-4}$ are 11.13 and 11.11 eV, respectively. These values are very close to the experimental appearance energy of $N(H_2O)_{3-4}^+$. After the vertical ionization of the neutral water sub-clusters, the water sub-cluster structure undergoes rearrangement, generating a proton-transfer like structure with OH radical bonded to the naphthalene. As can be seen from the Figure 11(a), the distance between the naphthalene carbon and the oxygen of the OH is 1.487 Å, while the distance between the oxygen and the remaining proton is 1.407 Å. Evidently OH addition to naphthalene has occurred, as this distance is longer than that of a typical single hydrogen bond. The proton attaches to the second oxygen at a distance of 1.063 Å. A similar picture can be seen for the case of 4 water molecules (Figure 11b); the distance between the carbon of naphthalene and the oxygen of the OH moiety is 1.473 Å, and the distance between the oxygen and the proton is 1.518 Å. The distance between the proton and the nearest water molecule in the cluster is 1.022 Å. These structures reveal an interesting charge-spin separation characteristic of distonic ions. A Mulliken analysis performed on the above cations reveals that while the charge of the cluster is mostly located on the water sub-cluster (0.75 a.u. and 0.81 a.u. for the 3 and 4 water clusters respectively) the spin is on the naphthalene moiety in both cases.

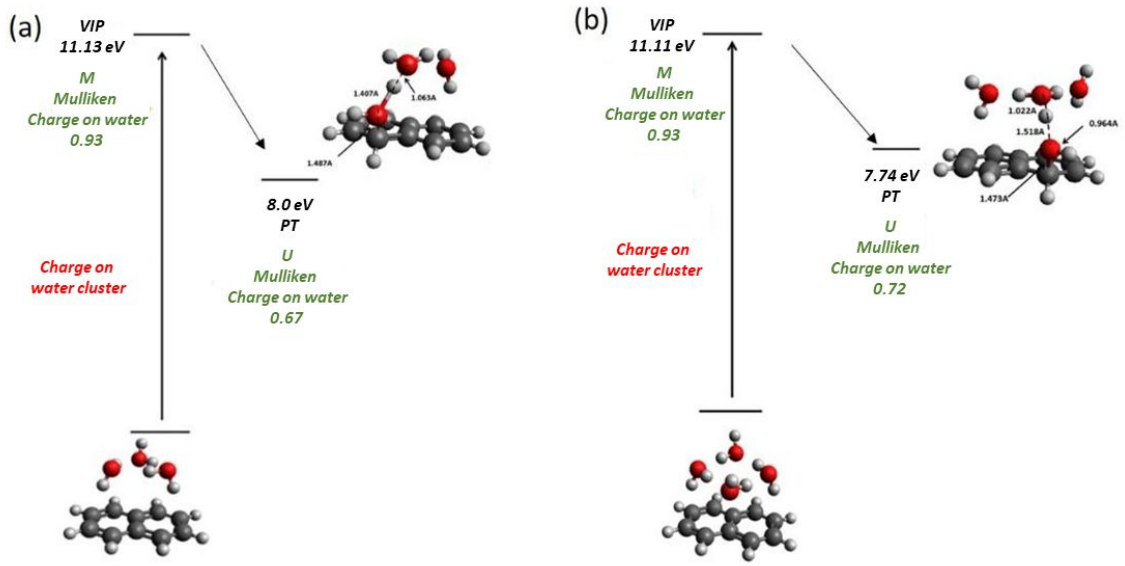

Figure 11. Ionization of water sub-clusters in $N(H_2O)_3$ and $N(H_2O)_4$.

Infrared-vacuum ultraviolet (IR-VUV) spectroscopy could be utilized to characterize the structures of these neutral and cationic $N(H_2O)_n$ clusters.[57] Since the vertical ionization energies of $N(H_2O)_x$ are around 11 eV, a VUV light source with tunable wavelength and intense pulse energy would be required to selectively ionize a given neutral cluster. The newly-built Dalian Coherent Light Source facility,[58-59] which delivers VUV free electron laser light with a continuously tunable wavelength region between 8-3-24.8 eV and high pulse energy, would be helpful for spectroscopic study on the naphthalene-water clusters with a broad range of ionization energies.

4. Intermolecular interactions in the ionized clusters.

As demonstrated in the calculated structures presented in Figure 4, ionized naphthalene water clusters can exhibit different binding patterns; here we investigate the aforementioned "top" and "side" configurations. In the "top" configuration, the interaction is mainly between hydrogens of the water and the π cloud of the naphthalene, while in the "side" configuration, the interaction is between the oxygen of the water and the hydrogens of the naphthalene. Alterations in binding patterns between these two configurations result from different driving forces. In order to further study, the difference between the two charged orientations, we performed energy decomposition analysis (EDA), [38-39, 60-63] and followed the scheme described in ref. 63 by Horn et. al. EDA is a valuable method for discerning the types of interactions present in a fragment system. Typical energy contributions are parsed into three major terms: electrostatic interaction, repulsive Pauli exchange, and covalent interactions.[39] The relative contributions of each component are indicative of the main forces contributing to bonding between fragments – here, interactions between naphthalene-water or within the water sub-clusters – and may provide further explanation for binding patterns within the two different configurations observed in these systems.

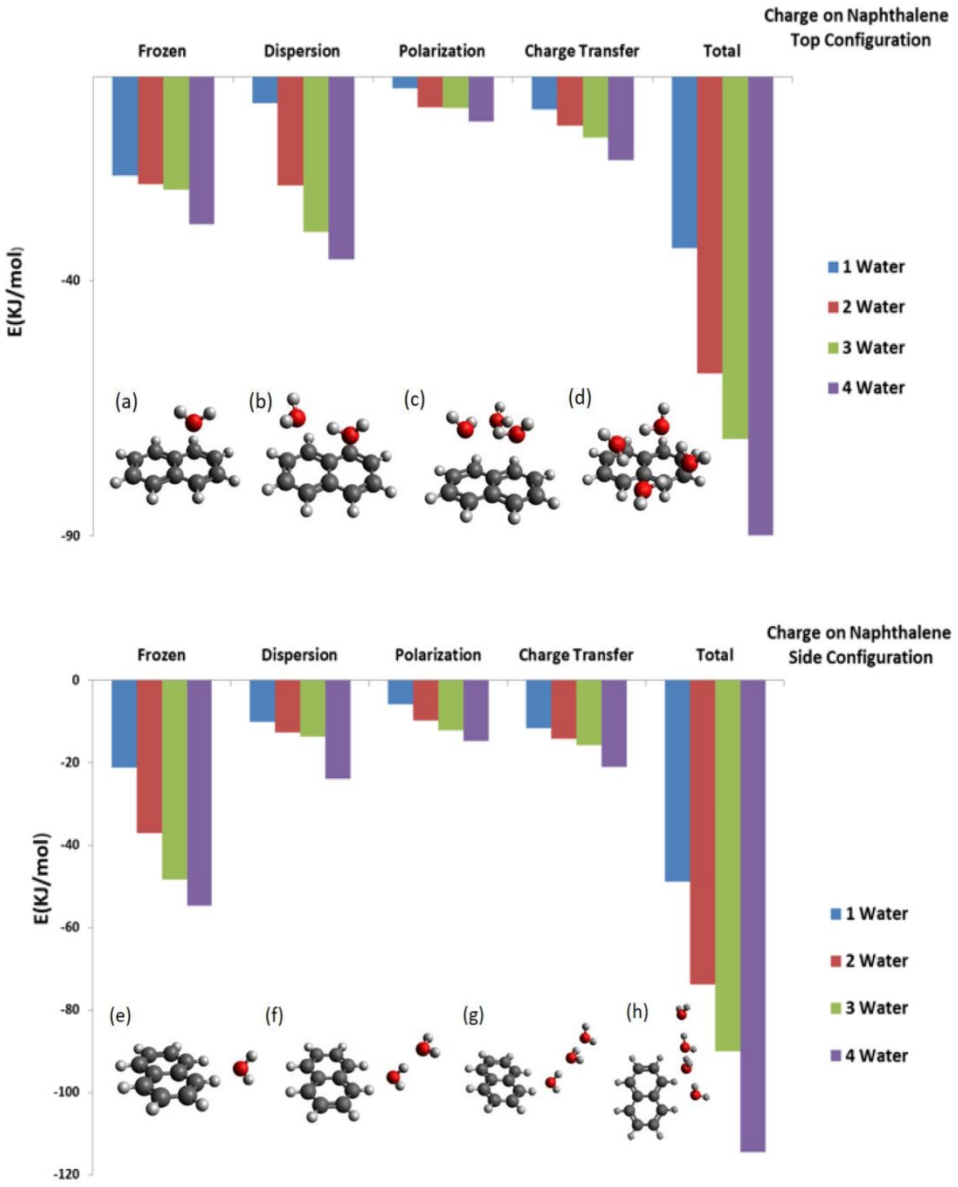

Figure 12. Energy decomposition analysis for naphthalene water complex. Top panel: Top configuration. Bottom panel: Side configuration.

Figure 12 presents the different components of the energy for the case of top (top panel) and side configuration (bottom panel). The Figure reveals different driving forces of the interaction for each of the configurations. For the "top" configuration, the largest contribution comes from the dispersion interaction, followed by frozen and charge transfer interactions (with the exception of the one water case). In the "side" configuration the dominant contribution is due to the frozen interaction, which results from electrostatics and indicates a strong charge dipole interaction,

with similar contributions from dispersion and charge transfer interactions. The more prominent role of permanent electrostatics in the "side" configurations is consistent with the linear chains of water generating a large dipole moment to couple to the charge of ionized naphthalene.

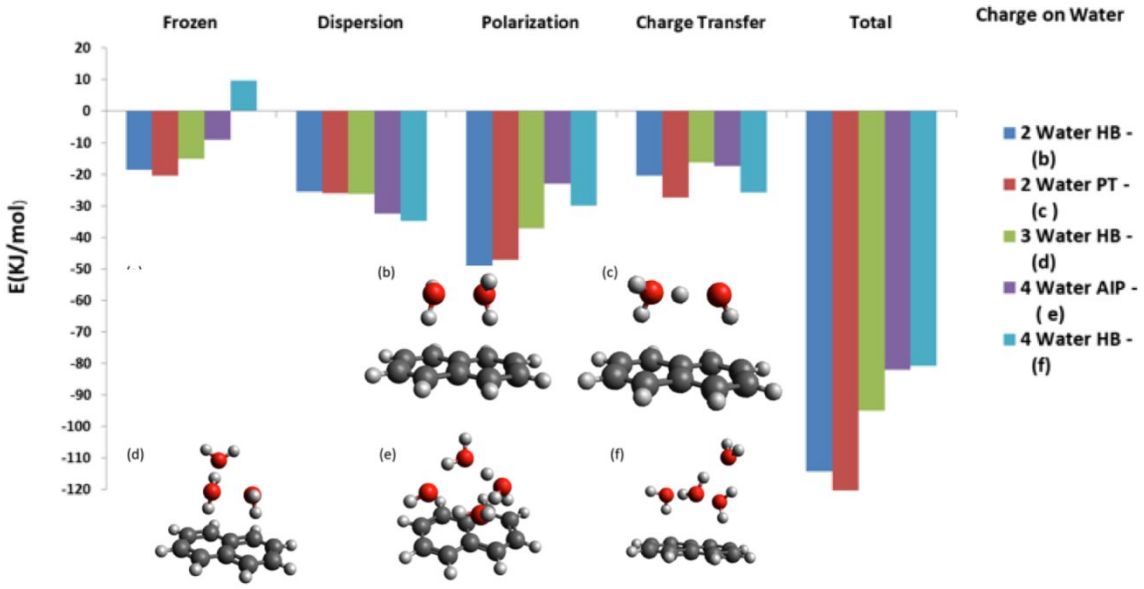

Figure 13. Energy decomposition analysis for naphthalene water complexes in the case where the charge is on the water moiety.

A similar analysis performed for the case where the charge is on the water sub-cluster, as shown in Figure 13. Here we see again contributions to the total energy divided into different terms, and we observe significant contributions from polarization, charge transfer, dispersion and frozen interaction. The leading contributions arise from polarization and dispersion interactions. For the case of two and three water molecules, the dominant term is the polarization term, while for the case of four water molecules the leading term is the dispersion term. Contributions from frozen and charge transfer are the smallest, although for the case of four water molecules, contribution from charge transfer becomes larger, while contribution from the frozen interaction becomes smaller. In this case, where the charge resides on the water sub-cluster, comparing Figure 13 with Figure 12 reveals that the polarization interaction becomes much more significant than the case where the charge resides on the naphthalene. This can be attributed to the induced response of the aromatic (π) cloud to the charge on the water sub-cluster. A second major difference between ionization on naphthalene (Figure 12) and ionization on the water cluster (Figure 13) is that the

total binding energy trends lower with larger numbers of water molecules in Fig. 13, while it trends higher in Fig. 12. This shows that the strongest interactions in the case of ionization on water are within the water sub-cluster for the cases shown in Fig. 13 (i.e. excluding hydroxyl attack on naphthalene!), while, by necessity, they are between ionized naphthalene and the water cluster in Fig. 12.

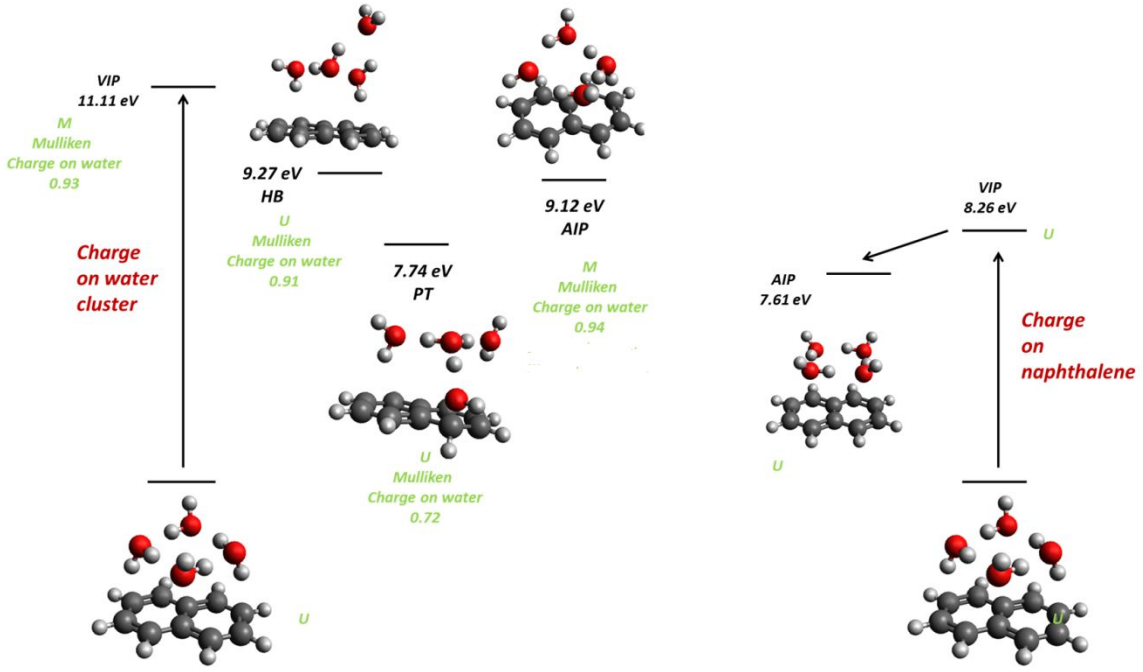

Figure 14. Left: ionization of the water sub cluster. Right: Channels upon ionization of the naphthalene part of the cluster.

5. Conclusion

Photoionization of naphthalene-water clusters is studied using a combined experimental and theoretical approach. Our study shows different channels of ionization of the naphthalene-water clusters dependent on energy of the ionizing photon. Figure 14 summarizes the results presented in this paper for the case of 4 water molecules, where ionization from either naphthalene or the water sub-cluster leads to different dynamics. The vertical ionization energy when naphthalene is being ionized is 8.26 eV, agreeing well with an experimental appearance energy of 8.2 eV. When the photon energy is below the water ionization threshold, the naphthalene moiety of the cluster

is ionized and no protonated naphthalene water clusters are observed. Rearrangements of the water sub-cluster upon ionization enhance their charge dipole interactions and other induced interactions with cationic naphthalene while maintaining the hydrogen bonding network. In the case for the water sub-cluster ionization, the calculated vertical ionization energy is 11.11eV, this agrees well with the experimental appearance energy of protonated naphthalene water clusters at around 11 eV. When ionization occurs above the water ionization threshold, there is proton transfer within the water-sub-cluster and hydroxyl radical emission. In addition, the generated hydroxyl radical can also react with naphthalene to form an adduct, and the proton is solvated by the other remaining waters. Energy decomposition analysis is used to shed light on the forces that are at play when charge is located in different parts of the naphthalene water system. This work provides an glimpse into the interactions of a 2 membered polycyclic hydrocarbons with small water clusters. In the future, we plan to embed larger PAH's into water clusters to truly mimic astrochemical icy surfaces and perhaps also explore water confinement within these hydrocarbons. Experiments probes, such as infrared spectroscopy, in conjunction with VUV photoionization will perhaps enable capturing some of the transient species that have been discovered theoretically here.

Acknowledgments:

This work was supported by the Director, Office of Science, Office of Basic Energy Sciences, of the U.S. Department of Energy (DOE) under Contract No. DE-AC02-05CH11231, through the Gas Phase Chemical Physics Program of the Chemical Sciences Division. The ALS is also supported via the same contract. TS, JH and MHG acknowledge additional partial support from the National Aeronautics and Space Administration (NASA) through the NASA Astrobiology Institute under Cooperative Agreement Notice NNH13ZDA017C issued through the Science Mission Directorate.

6. References

1. K. I. Oberg, *Chem. Rev.*, 2016, **116**, 9631-9663.
2. S. H. Cuylle, L. J. Allamandola and H. Linnartz, A&A, 2014, **562**, A22.
3. M. P. Bernstein, S. A. Sandford, L. J. Allamandola, J. S. Gillette, S. J. Clemett and R. N. Zare, *Science*, 1999, **283**, 1135-1138.
4. M. S. Gudipati, *J. Phys. Chem. A*, 2004, **108**, 4412-4419.

5. P. P. Bera, T. Stein, M. Head-Gordon and T. J. Lee, *Astrobiology*. **2017** *17*(8), 771-785.
6. M. Mons, I. Dimicoli and F. Piuzzi, *Int. Rev. Phys. Chem.*, 2010, **21**,101-135.
7. M. Miyazaki, A. Fujii, T. Ebata and N. Mikami, *J. Phys. Chem. A*, 2004, **108**, 10656 -10660.
8. M. Miyazaki, A. Fujii, T. Ebata and N. Mikami, *Chem. Phys. Lett.*, 2004, **399**, 412-416.
9. M. Miyazaki, A. Fujii and N. Mikami, *J. Phys. Chem. A*, 2004, **108**, 8269-8272.
10. M. Prakash, K. G. Samy and V. Subramanian, *J. Phys. Chem. A*, 2009, **113**, 13845-13852.
11. Y. M. Ibrahim, M. M. N. Mautner, E. H. Alshraeh, M. S. El-Shall and S. Scheiner, *J. Am. Chem. Soc.* 2005, **127**, 7053-7064.
12. P. M. Palmer and M. R. Topp, *Chem. Phys.*, 1998, **239**, 65-81.
13. J. Hernandez-Rojas, F. Calvo, F. Rabilloud, J. Breton and J. M. G. Llorente, *J. Phys. Chem. A*, 2010, **114**, 7267-7274.
14. A. L. Steber, C. Pérez, B. Temelso, G. C. Shields, A. M. Rijs, B. H. Pate, Z. Kisiel and M. Schnell, *J. Phys. Chem. Lett*, 2017, **8**, 5744-5750.
15. A. K. Lemmens, S. Gruet, A. L. Steber, J. Antony, S. Grimme, M. Schnell and A. M. Rijs, *Phys. Chem. Chem. Phys.*, 2018.
16. I. K. Attah, S. P. Platt, M. Meot-Ner, M. S. El-Shall, S. G. Aziz and A. O. Alyoubi, *Chem. Phys. Lett.*, 2014, **613**, 45-53.
17. V. Le Page, Y. Keheyan, T. P. Snow and V. M. Bierbaum, *J. Am. Chem. Soc.*, 1999, **121**, 9435-9446.
18. I. Alata, M. Broquier, C. Dedonder-Lardeux, C. Jouvet, M. Kim, W. Y. Sohn, S. S. Kim, H. Kang, M. Schutz, A. Patzer and O. Dopfer, *J. Chem. Phys*, 2011, **134**, 074307.
19. K. Chatterjee and O. Dopfer, *Phys. Chem. Chem. Phys.*, 2017, **19**, 32262-32271.
20. K. Chatterjee and O. Dopfer, *Chem. Sci.*, 2018, **9**, 2301-2318.
21. E. A. Cabaleiro-Lago, J. Rodriguez-Otero and A. Pena-Gallego, *J. Phys. Chem. A*, 2008, **112**, 6344-6350.
22. D. Sharma and M. J. Paterson, *RSC Adv.*, 2015, **5**, 28281-28291.
23. P. Hirunsit and P. B. Balbuena, *J. Phys. Chem. A*, 2007, **111**, 10722-10731.
24. S. McKenzie and H. C. Kang, *Phys. Chem. Chem. Phys.*, 2014, **16**, 26004-26015.
25. B. Radha, A. Esfandiar, F. C. Wang, A. P. Rooney, K. Gopinadhan, A. Keerthi, A. Mishchenko, A. Janardanan, P. Blake, L. Fumagalli, M. Lozada-Hidalgo, S. Garaj, S. J. Haigh, I. V. Grigorieva, H. A. Wu and A. K. Geim, *Nature*, 2016, **538**, 222-225.
26. O. Dopfer and M. Fujii, *Chem. Rev.*, 2016, **116**, 5432-5463.

27. L. M. Salonen, M. Ellermann and F. Diederich, *Angew. Chem. Int. Ed.*, 2011, **50**, 4808-4842.
28. M. S. Gudipati and L. J. Allamandola, *Astrophys. J.*, 2004, **615**, L177-L180.
29. D. E. Woon and J. Y. Park, *Astrophys. J.*, 2004, **607**, 342-345.
30. Y. Keheyan and I. L. ten Kate, *Orig. Life Evol. Biosph.*, 2012, **42**, 179-186.
31. K. Khistyaev, K. B. Bravaya, E. Kamarchik, O. Kostko, M. Ahmed and A. I. Krylov, *Faraday Discuss.*, 2011, **150**, 313-330.
32. Y. Shao, et al., *Mol. Phys.* 2015**, 113**, 184-215.
33. N. Mardirossian and M. Head-Gordon, *Phys. Chem. Chem. Phys.*, 2014, **16**, 9904-9924.
34. E. Livshits, R. S. Granot and R. Baer, *J. Phys. Chem. A*, 2011, **115**, 5735-5744.
35. O. A. Vydrov and T. V. Voorhis, *J. Chem. Phys.*, 2010, **133**, 244103.
36. N. Mardirossian and M. Head-Gordon, *Mol. Phys.*, 2017, **115**, 2315-2372.
37. N. Mardirossian and M. Head-Gordon, *J. Chem. Phys.* 2018, **148**, 241736.
38. R. Z. Khaliullin, M. Head-Gordon and A. T. Bell, *J. Chem. Phys.* 2006**, 124** (20), 204105.
39. P. R. Horn, E. J. Sundstrom, T. A. Baker and M. Head-Gordon, *J. Chem. Phys.* 2013**, 138** (13), 134119.
40. H. Stoll, G. Wagenblast and H.Preuβ, *Theor. Chim. Acta.* 1980**, 57** (2), 169-178.
41. A. T. B. Gilbert, N. A. Besley and P. M. W. Gill, *J. Phys. Chem. A* 2008**, 112** (50), 13164-13171.
42. L. Belau, K. R. Wilson, S. R. Leone and M. Ahmed, *J. Phys. Chem. A*, 2007, **111**, 10075-10083.
43. T. Yang, T. P. Troy, B. Xu, O. Kostko, M. Ahmed, A. M. Mebel and R. I. Kaiser, *Angew. Chem. Int. Ed.*, 2016, **55**, 14983-14987.
44. T. Fujiwara and E. C. Lim, *J. Phys. Chem. A*, 2003, **107**, 4381-4386.
45. P. M. Palmer and M. R. Topp, *Chem. Phys.*, 1998, **239**, 65-81.
46. A. Courty, M. Mons, I. Dimicoli, F. Piuzzi, M.-P. Gaigeot, V. Brenner, P. de Pujo and P. Millié, *J. Phys. Chem. A*, 1998, **102**, 6590-6600.
47. T. K. Ghanty and S. K. Ghosh, *J. Phys. Chem. A* **2002,** *106* (48), 11815-11821.
48. M. Sodupe, J. Bertran, L. Rodríguez-Santiago and E. J. Baerends, *J. Phys. Chem. A* 1999, **103** (1), 166-170.
49. M. Sodupe, A. Oliva and J. Bertran, *J. Am. Chem. Soc.* 1994, **116** (18), 8249-8258.

50. P. A. Pieniazek, J. VandeVondele, P. Jungwirth, A. I. Krylov and S. E. Bradforth, *J. Phys. Chem. A* 2008, **112** (27), 6159-6170.

51. T. Stein, C. A. Jiménez-Hoyos and G. E. Scuseria, *J. Phys. Chem. A* 2014, **118** (35), 7261-7266.

52. A. Courty, M. Mons, J. Le Calvé, F. Piuzzi and I. Dimicoli, *J. Phys. Chem. A*, 1997, **101**, 1445-1450.

53. K. Khistyaev, A. Golan, K. B. Bravaya, N. Orms, A. I. Krylov and M. Ahmed, *J. Phys. Chem. A*, 2013, **117**, 6789-6797.

54. K. Lorenz and R. Zellner, *Ber. Bunsenges. Phys. Chem*, 1983, **87**, 629-636.

55. R. Atkinson and J. Arey, *Polycycl. Aromat. Compd.*, 2007, **27**, 15-40.

56. M. Gnanaprakasam, L. Sandhiya and K. Senthilkumar, *Theor. Chem. Acc.*, 2017, **136**, 131.

57. Y. Matsuda, N. Mikami and A. Fujii, *Phys. Chem. Chem. Phys.*, 2009, **11**, 1279-1290.

58. D. Normile, *Science*, 2017, **355**, 235-235.

59. Y. Chang, S. Yu, Q. Li, Y. Yu, H. Wang, S. Su, Z. Chen, L. Che, X. Wang, W. Zhang, D. Dai, G. Wu, K. Yuan and X. Yang, Rev. Sci. Instrum., 2018, **89**, 063113

60. R. Z. Khaliullin, A. T. Bell and M. Head-Gordon, *J. Chem. Phys.* 2008, **128** (18), 184112.

61. R. Z. Khaliullin, E. A. Cobar, R. C. Lochan, A. T. Bell and M. Head-Gordon, *J. Phys. Chem. A* 2007, **111**, 8753-8765.

62. J. Thirman, E. Engelage, S. M. Huber and M. Head-Gordon, *Phys. Chem. Chem. Phys.* 2018, **20**, 905-915.

63. P. R. Horn, Y. Mao and M. Head-Gordon, *J. Chem. Phys.* 2016, **144** (11), 114107.

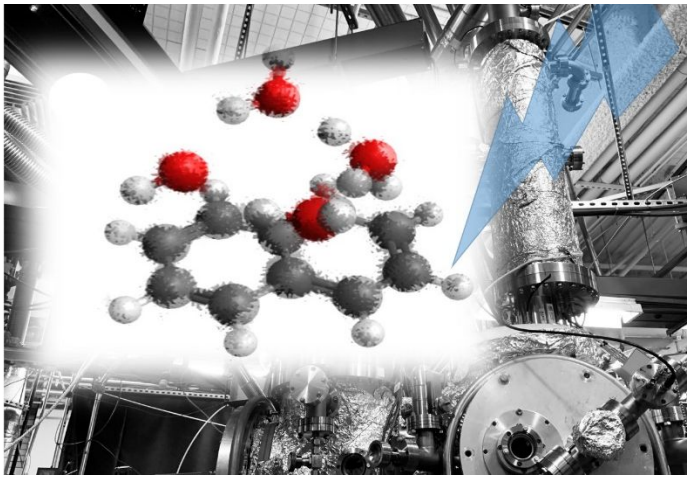

TOC entry

Synchrotron based mass spectrometry coupled with theoretical calculations provide insight into polycyclic aromatic hydrocarbon water interactions.